Volume 1 | Number 1 | Jan 2013 | Pages 1–100

Nanoscale

www.rsc.org/nanoscale

ROYAL SOCIETY OF CHEMISTRY

www.rsc.org/nanoscale

Journal Name

ARTICLE

Asymmetric AgPd-AuNR heterostructure with enhanced photothermal performance and SERS activity

Han Zhang,[a] Zeke Liu,[b] Xiaolin Kang,[a] Jun Guo,[c] Wanli Ma,[b] and Si Cheng*[a]

Most of as-reported nanostructures through galvanic replacement reaction are still symmetric hollow structures till now. Asymmetric structure fabricated through galvanic replacement reaction has been rarely reported. However, asymmetric heterostructures can generally lead to new intriguing properties through asymmetric synergistic coupling. Here, we report a simple synthesis of asymmetric one-ended AgPd bimetal on Au nanorods (AuNR) by combining galvanic replacement reaction and Ostwald ripening process. The morphological evolution from nanodumbbell to dandelion structure is thoroughly investigated. The unique asymmetric AgPd-AuNR heterostrcture possess required plasmonic performance and avoids strong damping caused by poor plasmonic metal Pd, resulting in superior photothermal heating performance and enhanced SERS sensitivity for in situ monitoring catalytic reaction compared with symmetric counterparts.

Introduction

Galvanic replacement reactions provide a particularly facile and versatile route to create geometry-dependent heterogeneous nanostructures,[1] and the resultant shapes of the nanostructures by galvanic replacement are very sensitive to the reaction conditions, the metal type and the crystalline structure of the seed nanocrystals.[1a, 1d] It has been reported that small changes in the reaction conditions of galvanic replacement on Ag nanocubes led to different morphologies.[1e,2] However, most of as-reported nanostructures through galvanic replacement reaction are still symmetric hollow structures till now.[1a,1f,2a,2d] Asymmetric structure fabricated through galvanic replacement reaction has been rarely reported. Asymmetric heterostructures can lead to new intriguing properties through drastically combining different chemical or physical properties within a single particle since each counterpart can provide surface functional moieties with asymmetric synergistic coupling.[3] To date, engineering asymmetric metal heterostructure is still a considerable challenge although many efforts have been paid over the past few years,[3a, 3e,3f] because symmetric structures exhibit more stable state or lower energy barrier than asymmetric structures and breaking the symmetrical obstacle of nanoparticles at the nanoscale is difficult yet.[3a, 3d, 3e] For example, Pd or Pt generally deposits on Au nanocrystals to form symmetric nanodumbbell or core-shell Au-Pd or Au-Pt nanostructures.[4] Therefore, developing a novel approach for fabricating asymmetric heterostructures would offer new horizons for diverse functionalities of metal nanoparticles (NPs).

In our previous research, we prepared Au bipyramids (AuBPs)/AgPd nanodumbbell nanoparticles through galvanic replacement.[1b] AgPd nanodendrites can be symmetrically coated on the end of AuBPs. Nanodendrites nanostructures generally show improved catalytic property compared to their solid counterparts owing to higher surface to volume ratio and the presence of a large number of active atoms on the edges, corners, or defects on the surface of the nanoparticles.[4c,4e-g] However, the symmetrical AgPd coating resulted in strong damping of the plasmon resonances of AuBPs,[1b,] which severely suppresses the plasmonic property of AuBPs. Here, we report the growth process of one-ended AgPd bimetal on AuNR through combining galvanic replacement reaction and Ostwald ripening. By simply controlling the reaction conditions, the shape of NPs can be changed from nanodumbbell to dandelion and solid lollipop structure (Figure 1.). Importantly, this distinctive dandelion structure possesses intriguing dual functionality. One-ended growth of AgPd nanodendrites offers abundant catalytic sites, whereas uncoated AuNR on the other end of dandelion structure continues to preserve required plasmonic performance, which is unavailable for symmetric nanodumbbell counterpart. Furthermore, dandelion NPs were demonstrated enhanced photothermal heating performance and SERS activity over nanodumbbell NPs.

Results and discussion

Our strategy for the preparation of nanodumbbell, dandelion and lollipop structure was shown in Figure 1. For a

a. College of Chemistry, Chemical Engineering and Materials Science, Soochow University, Suzhou, Jiangsu, 215123, China. E-mail: chengsi@suda.edu.cn
b. Institute of Functional Nano & Soft Materials (FUNSOM), Soochow University, Suzhou, Jiangsu, 215123, China
c. Testing & Analysis Center, Soochow University, Suzhou, Jiangsu, 215123, China
†Electronic Supplementary Information (ESI) available: [details of any supplementary information available should be included here]. See DOI: 10.1039/x0xx00000x

standard synthesis process, we started using a AuNRs sample with an average length/diameter of (78.2 ± 4.4)/(17.9 ± 1.1) nm, which exhibits a longitudinal plasmon resonance at 823 nm (Figure S1). The AuNR@Ag nanorods were grown according to the procedure described previously.[5] Ag preferred to grow at the sides of nanorods and the Ag shells at the side of the nanorods are seen to be thicker than those at the ends. The width of AuNR@Ag nanorods varied from 28.3±1.3 nm to 45.9±3.1 nm as the volume of AgNO$_3$ increased from 60 µL to 500 µL (Figure S2). The extinction spectra of the AuNR@Ag samples are shown in Figure S3, which are consistent with the previous report.[5] Afterwards, 40 µL of H$_2$PdCl$_4$ solution and 20 µL of ascorbic acid (AA) were added into the AuNR@Ag solution.
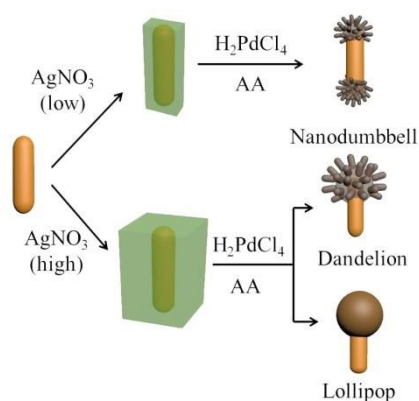

Figure 1. Schematic illustration of the formation of nano-dumbbell, dandelion and lollipop nanostructure.

Interestingly, we found that nanodumbbell structure was obtained when the volume of AgNO$_3$ was less than 400 µL (Figure 2a and Figure S4a-d). However, with an increase in volume to 400 µL for AgNO$_3$, a small number of one-ended growth of nanodendrites on AuNR (dandelion structure) began to appear (Figure S4e). Further increasing the volume of AgNO$_3$ to 500 µL, a large number of dandelion structures can be obtained (Figure 2b and Figure S4f). The TEM images reveal the Au core and well-defined nanodendrites shell consisting of numerous tiny interconnected nanoarms in nanodumbbell and dandelion structure. Moreover, when the amount of AA increased, these nanodendrites disappeared and a solid one-ended structure (lollipop structure) appeared (Figure 2i-l). High-angle annular dark-field scanning transmission-electron microscopy (HAADF-STEM) and corresponding elemental mappings show that Ag and Pd are uniformly distributed in these structures (Figure 2b,f,j). The lattice fringes ascribed to (111) and (200) planes of Pd and Ag are clearly observed in HRTEM images recorded on the individual nanostructure (Figure 2d,h,l). The SEAD patterns of nanodumbbell, dandelion and lollipop nanostructures exhibit polycrystalline diffraction rings (Figure S5), indicating that the AgPd nanodendrites are polycrystalline structures. The products were then examined by the X-ray photoelectron spectroscopy (XPS) study (Figure S6). The XPS full-scan spectrum of the dandelion and nanodumbbell samples dominated the existence of Au, Ag and

Pd (Figure S6a and e). Figure S6b-d and f-h present the high-resolution XPS spectra of Au, Ag and Pd. The Au 4f$_{5/2}$ and 4f$_{7/2}$ peaks of dandelion NPs are observed at 83.62 and 87.32 eV. The Au 4f$_{5/2}$ and 4f$_{7/2}$ peaks of nanodumbbell NPs are observed at 83.52 and 87.22 eV, respectively. Four peaks, 373.52/367.55 eV in Figure S6c and 373.43/367.42 eV in Figure S6g can be observed in the Ag 3d spectrum, which can be assigned to the Ag 3d$_{3/2}$ and 3d$_{5/2}$ of metallic silver, respectively. [6] The XPS spectra of Pd 3d show asymmetric signals, indicating there are multiple palladium species on the surface. The Pd 3d peaks of dandelion and nanodumbbell NPs can be deconvoluted into four peaks which can be associated to 3d$_{5/2}$ and 3d$_{3/2}$ signals of elemental palladium,[6a-c] indicating that Pd is present as mainly Ag/Pd alloys and little metallic Pd. The metallic Pd existence may be due to the additional AA for co-reduction reaction since the growth of Pd in CTAC solutions is very fast.[7] In addition, the binding energies of Ag and Pd show negative shifts compared to those of pure atomic Ag and Pd, further demonstrating the existence of AgPd alloys.[6] Figure S7 shows the X-ray Diffraction (XRD) patterns of the as-synthesized nanodumbbell and dandelion NPs, from which five strong diffraction peaks could be indexed to the (111), (200), (220), (311) and (222) plane of the samples. Compared to the patterns of bulk Au, Ag and Pd from the Joint Committee on Powder Diffraction Standards (JCPDS), the diffraction peaks of the synthesized samples are located between the peaks of pure Pd and Ag, further indicating the formation of AgPd alloys, which is consistent with the previous reports that Pd atoms can diffuse into Ag to form a alloyed crystal structure during galvanic replacement reaction.[6]
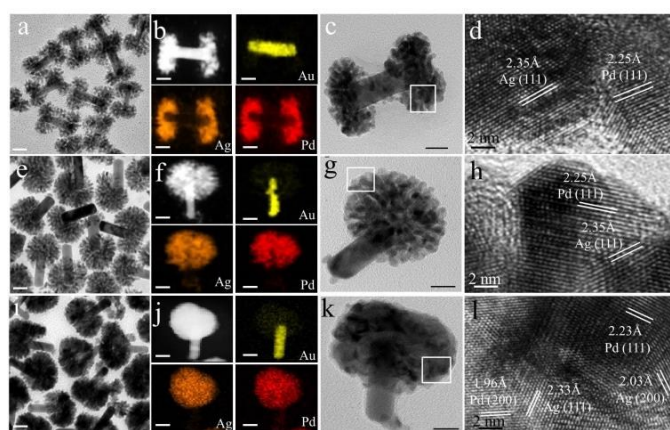

Figure 2. TEM, HAADF-STEM EDS elemental mapping and HRTEM images of nanodumbbell (a-d), dandelion (e-h) and lollipop structures (i-l). Scale bar: 20 nm

We investigated the role of AA and cetyltrimethylamonium chloride (CTAC) in affecting the galvanic replacement reaction between Ag and H$_2$PdCl$_4$ solution and thereby the morphological development. Specifically, keeping the amount of AgNO$_3$ constant (500 µL), we performed a set of experiments to monitor the morphology evolution by modulating the volume of AA and CTAC (Figure 3). If no AA and CTAC were added into AuNR@Ag solution, AuNR@AgPd core-shell

structures were observed (Figure 3a). At the same time, some nanoparticles with excess Ag were not totally replaced by Pd (Figure S8a), indicating that the galvanic re-placement reaction is incomplete. Only increasing the amount of AA resulted in more solid AgPd bimetal on AuNR and no dandelion NPs were observed (Figure 3b-c and Figure S8b-c). Similarly, no dandelion structures appeared when merely improving the volume of CTAC (Figure S8e-g). Surprisingly, after additional 30 μL of CTAC and 20 μL of AA solution simultaneously, the dandelion structures began to appear along with a few of nanodumbbell nanoparticles (Figure 3e and Figure S9a). Solid lollipop structures were further obtained as the volume of AA reached to 60 μL (Figure 3f, FigureS9b). Continuing to increase the volume of CTAC to 60 μL, a large number of dandelion structures was obtained (Figure 3h and S9c).
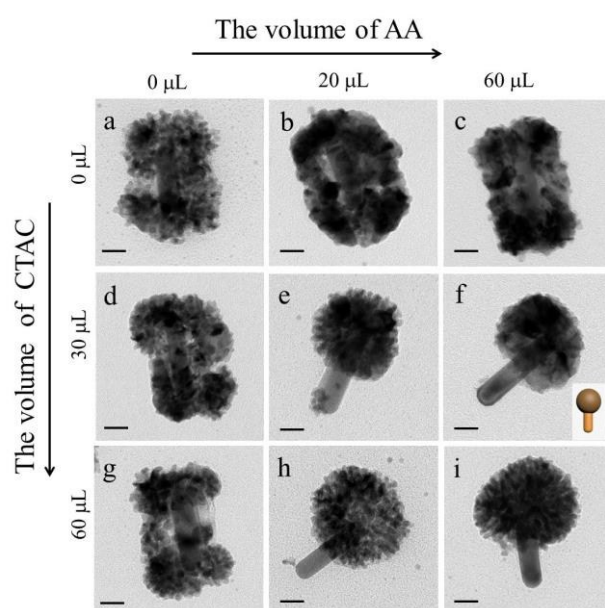

Figure 3. Morphologies evolution process as a function of the volume of CTAC and AA. The volume of AgNO$_3$ is 500 μL. See SI for supplementary TEM. Scale bar: 20 nm.

The above results imply that the coordinated use of both CTAC and AA is essential for the formation of dandelion structures. Usually, halide ions are used to bind with Ag$^+$ ion and drives down the reduction potential of Ag$^+$/Ag, favouring the oxidation of Ag^0 by Au^{3+} or Pd^{2+} or Pt^{4+}.[8] In addition, the growth of Pd in CTAC solutions is very fast and dendrite Pd NPs are obtained from the growth with Cl-.[7] The co-reduction using AA as the reductant also boosted the reduction proceeding,[1b, 8b] but excess AA would also induce the distinct morphological transition from nanodendrites NPs into solid ones. However, it is noteworthy that if the volume of AgNO$_3$ is low(<400 μL), improving the volume of AA would not result in the morphology transition from nanodumbbell to dandelion structure but more solid AgPd dumbbell structures (Figure S10). Similarly, no dandelion structures appeared when merely increasing or decreasing the volume of H$_2$PdCl$_4$ when the volume of AgNO$_3$ is <400 μL (Figure S11a-d). However, the content of the Pd precursor has more influences on the

morphological evolution of NPs when the volume of AgNO$_3$ reached to 500 μL (Figure S11e-h). Low H$_2$PdCl$_4$ volume resulted in incomplete galvanic replacement and a large amount of Ag was not replaced (Figure S11e-f). With an increased H$_2$PdCl$_4$ volume of 40-60 μL, a well-defined dandelion structure can still be obtained (Figure S11g). However, too much Pd precursor content (80μL) would get rise to solid AgPd structures (Figure S11h) and some AgPd bimetal would fall off from the gold nanorods due to the excessive consumption of Ag.[1b] These results illustrate that the content of Ag/Pd ratio play a crucial role on the growth of dandelion structure. The high relative ratios of Ag to Pd will be prone to the formation of dandelion structures.[3d]
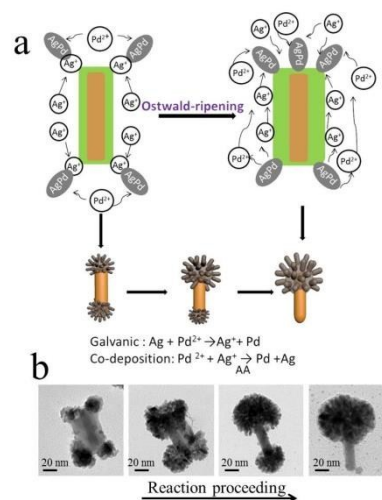

Figure 4. a) Schematic illustration of a plausible mechanism for the morphology evolution process. b) Representative TEM images of the products formed at different stages in the course of galvanic reaction and Ostwald ripening.

Meanwhile, a plausible mechanism was proposed to explain above morphology evolution. We speculate that the electron released by the galvanic oxidation of the Ag shell travelled to and accumulated at the end of corners because of the high curvatures and a low coverage density for the capping agent there.[1c, 9] Then the Pd precursor would be reduced and deposited preferentially on these electron-rich region accompanying with the Ag on the side of AuNR being gradually consumed,[1c, 9] which may be responsible for the formation of nanodumbbell structures (Figure 4 and Figure S12)). For the AuNRs@Ag samples with thick Ag shell, more Ag^0 were oxidized by Pd^{2+} to Ag$^+$ as the galvanic replacement proceeded, relative with those samples with thin Ag shell. As the Ag$^+$ concentration increased, Ostwald ripening effect during the galvanic replacement coupling co-reduction process will drive AgPd from one end to the other, resulting in the formation of the asymmetric one-ended AgPd growth behavior (Figure 4a). Ostwald ripening is a phenomenon that small nanoparticles dissolved and re-deposited onto larger particles,[10] which has been employed to explain the growth of Au nanoparticles at one tip of CdSe nanorods where ripening process drives gold

from one tip to the other when a higher relative ratio of gold to CdSe rods was used.[3d]

In general, too much Pd on AuNR leads to largely decreasing and broadening of plasmonic peak intensity of AuNRs due to strong damping caused by the large imaginary part of Pd dielectric function.[1b,3c,4d,11] We used UV-vis spectroscopy to elucidate the difference of optical properties of dandelion and nanodumbbell structure, as shown in Figure S13. It was found that the corresponding absorption spectrum of nanodumbbell NPs shows a significant damping of the peak feature, and the absorption band of AuNRs becomes completely featureless for nanodumbbell structure, whereas the dandelion NPs still show strong plasmon resonances peak. Moreover, the photothermal heating performances of gold nanorods, dandelion and nanodumbbell NPs were investigated. The Au mass concentrations of gold nanorods, dandelion and nanodumbbell NPs measured using inductively coupled plasma mass spec-trometry (ICP-OES) were synthetically controlled to be the same (Experiment sections). 2 mL aqueous solutions with or without metal NPs were illuminated by the 808 nm laser at 1.45 W respectively. The temperatures were recorded through an infrared (IR) thermal camera (Figure S15). The temperature rise traces under the laser illumination for the samples are provided in Figure 5a and Figure S14. The temperature of the solution containing metal NPs first increase rapidly and then reach their steady-state temperatures within 20 min. The final steady-state temperature for gold nanorods, dandelion NPs and nanodumbbell NPs are 88.9 ^{o}C, 86.2 ^{o}C and 66.3 ^{o}C, respectively, implying that the photothermal heating performance of dandelion NPs is superior to that of nanod-umbbell NPs. The final steady-state temperature of gold nanorods is slightly higher than that of dandelion NPs, but the dandelion NPs with AgPd nanodendrites will provide abundant catalytic sites in comparisons with pure gold nanorods. In addition, gold/Pd(Pt or Ag) bimetal or trimetallic heterostructures usually show enhanced catalytic activity compared to their monometallic counterparts, owing to the synergistic effect of multimetal.[4c,4e-h] Therefore, this excellent photothermal heating property accompanying with abundant catalytic sites offers a promising opportunity for dandelion structures to be widely used in plasmonic photocatalysis in the near future.

We also employed the application of dandelion structures for in situ SERS monitoring catalytic reaction. Applying SERS to *in situ* monitor catalytic reactions generally requires ap-propriate bifunctional nanoparticles which integrated re-markable plasmonic and catalytic activity.[12] In general, Pd exhibits remarkable catalytic activity, but shows extremely poor SERS activity.[4d] Depositing a thin layer of Pd on the surface of Au for the formation of bimetallic nanostructure with dual functionality is a general approach to integrate the catalytic and SERS properties on a single nanoparticle.[4d, 11c] Too thick Pd coating will result in largely decreasing of plasmon

peak intensity of Au, which severely suppresses the SERS activity.[3c,11] The unique morphology and composition of dandelion structures can avoid this problem. One-ended growth of AgPd nanodendrites offer abundant catalytic sites, whereas naked AuNR on the other end of nanostructure provided required plasmonic performance, making it useful for in situ monitoring a catalytic reaction via SERS. The SERS spectra of 4-nitrothiophenol indicated the stronger Raman signal on dandelion NPs compared to that on nanodumbbell NPs (Figure 5b).

As a proof-of-concept study, we employed these structures for monitoring of the reduction of 4-nitrothiophenol (4-NTP) to 4-aminothilphenol (4-ATP) at room temperature. First, the reduction reaction was per-formed by nanodumbbell NPs. The Raman signal by nanodumbbell NPs was very weak and apparent Raman peaks were rarely observed as the reaction proceeded (Figure S16). Next, we assessed the catalytic and SERS activity of dandelion structure using the same model reaction (Figure 6). We recorded the time-dependent SERS spectra of 4-NTP. At t=0, the SERS spectrum of the 4-NTP exhibited characteristic bands at 1109, 1335 and 1570 cm^{-1} that were respectively assigned to C–S stretching, O–N–O stretching, and the phenyl-ring mode.[12] As the reaction proceeded, the intensities of the R-NO$_2$ associated bands decreased with the conversion of 4-NTP to 4-ATP. Two new characteristic bands of 4-ATP at 1483 and 1594 cm^{-1} emerged, which are attributed to phenyl ring modes of 4-ATP (Figure 6b).[12b] This result confirmed that naked AuNR on the other end of dandelion structure plays an important role for SERS performance.
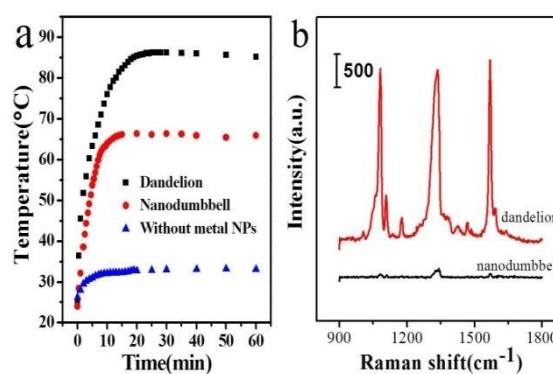

Figure 5. a) Temperature rise traces of the aqueous solutions at 1.45 W of the 808 nm laser. The black symbols are for the solution containing dandelion NPs, the red symbols are for the solution containing nanodumbbell NPs and the blue symbols are for the solution without metal NPs. b) Raman spectra of 4-NTP (1×10^{-4} M) adsorbed on dandelion and nanodumbbell nanoparticles.
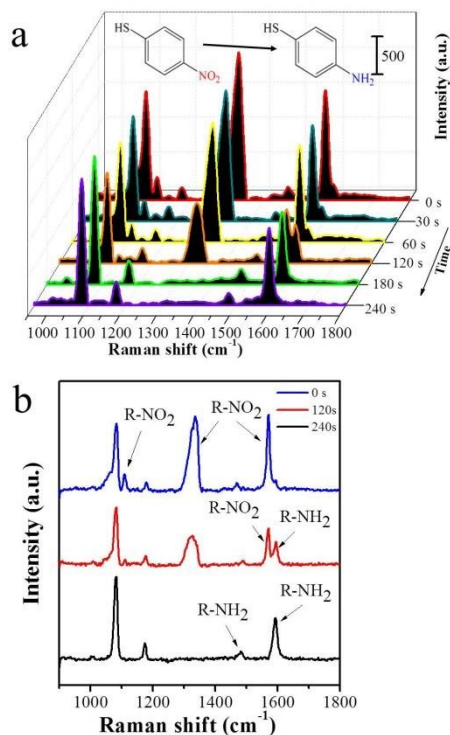
Figure 6. a) In situ Raman spectra of monitoring the reduction of 4-NTP to 4-ATP by dandelion NPs at different reaction time. b) SERS spectra of 4-NTP to 4-ATP at the initial stage (0 s), an intermediate stage (120 s) and at final stage (240 s).

Conclusions

In conclusion, we have reported a simple strategy to prepare asymmetric AgPd-AuNR heterostructure by combining galvanic replacement reaction and Ostwald ripening process. AgPd bimetal is site-specific grown on the one end of AuNR or on the two ends of AuNR through varying the amount of AgNO₃. Meanwhile, the one-ended AgPd bimetal can be tuned from nanodendrites (dandelion) to solid (lollipop) structure through tuning the amount of reductant. The intriguing dandelion structure ensure that AgPd nanodendrites on the one end of AuNR offer abundant catalytic sites while exposed Au on the other end of AuNR preserves required plasmonic performance. Our results show that the photo-thermal heating performance and SERS activity of dandelion NPs are superior to those of nanodumbbell NPs. We believe that our work offers a promising strategy and new horizons for design asymmetric heterostructures for diverse functionalities of metal NPs.

Experimental Section

Chemicals and materials: Chloroauric acid (HAuCl₄, >99.5%), palladium chloride powder (PdCl₂, 99%), and hydrochloric acid (HCl, 35%~36%) were all purchased from China Medicine (Group) Shanghai Chemical Reagent Corporation. L-Ascorbic acid (AA), silver nitrate (AgNO₃, 99%), sodium borohydride

(NaBH4, 99%), hexadecyl-trimethyl-ammonium bromide (CTAB) and cetyl-trimethyl-ammonium chloride (CTAC) were supplied by Sigma-Aldrich. All these were used as received. Ultra-filtered water (18.2 MΩ.cm) used in all reactions was obtained using a Millipore purification system (Simplicity).

Preparation of gold nanorods (AuNRs): The growth of AuNRs was based on previously reported procedures.[11a] Briefly, the seeds were first prepared by adding 0.250 mL of 0.01 M HAuCl₄ into 9.75 mL of 0.1 M CTAB, followed by the addition of ice-cold, freshly prepared NaBH₄ (0.01 M, 0.60 mL) under vigorous shaking. The resulting seed solution was kept standing at room temperature for at least 2 h before use. The nanorods growth solution was composed of 40 mL of 0.1 M CTAB, 2 mL of 0.01 M HAuCl4, 0.40 mL of 0.01 M AgNO₃, 0.80 mL of 1M HCl solution and 0.32 mL of 0.1 M ascorbic acid. 0.10 mL of the CTAB-stabilized seeds solution was then added into the growth solution, respectively. The reaction solution was mixed by gentle inversion for 10 s and then left undisturbed over-night at room temperature.

Preparation of AuNRs@AgPd nanodendrites nanostructures: The AuNRs@AgPd dumbbell and dandelion nanostructures were prepared in two steps. First, the AuNRs@Ag core-shell nanostructure was grown according to the reported recipe.[11a] Typically, 1 mL of AuNRs was centrifuged twice at 6500 rpm for 15 min and redispersed into CTAC solution (80 mM, 1 mL). Varying amounts of AgNO₃ (0.01 M) solution (60 μL, 100 μL, 200 μL, 300 μL, 400 μL, 500 μL) was subsequently added into the AuNRs-CTAC solution, followed by the addition of AA solutions (0.1 M). The volume of AA was varied to 15 μl, 25 μl, 40 μl, 75 μl, 100 μl, 125 μl respectively. And then, AuNRs@AgPd nanostructures were prepared by coupling galvanic replacement with a co-reduction process according to our previous report with some minor modifications.[1b] Briefly, 1 mL of the as-synthesized AuNRs@Ag solution was centrifuged twice at 6500 rpm for 15 min, redispersed into 1 mL of ultra-filtered water, followed by the addition of 40 μL of H₂PdCl₄ (0.01 M), 0-60μL of 80 mM CTAC, and 0-20 μL AA (0.01 M) solution. The resulting solutions were then left undisturbed for 1 h at room temperature.

Photothermal conversion: The mixture solution (2 mL) in the presence with DI water (1.5 mL) and the gold nanorods (0.5 mL), one-ended dandelion structure (0.5 mL) or two-ended nanodumbbell structure (0.5 mL) in a quartz cuvette with an optical path length of 1cm were exposed to the 808 nm NIR laser (Hi-Tech Optoelectronics Co., Ltd. Beijing, China) at the power density of 1.45 W/cm² for 1 h. For the control group, DI water (2 mL) without the nanoparticles was also kept under the illumination of the 808nm laser in the same condition. An infrared (IR) thermal camera was used to monitor the temperatures of the solutions during the photothermal process, which were imaged under a digital microscope (Leica Qwin). The concentrations of all nanoparticles were determined by ICP-OES to keep the number of Au atoms roughly on the same scale for all samples. The sample for ICP-OES was prepared by dissolving 1mL of nanoparticles in a mixture of hydrochloric acid (HCl, 36.5% in vol, 0.9 mL) and nitric acid (HNO₃, 70% in vol, 0.3 mL), followed by dilution with

ARTICLE

DI water until the volume of the final solution reached 25 mL. 0.5 mL of pure gold nanorods solution contained 7.2×10^{-2} mg Au, 0.5 mL of the dandelion nanostructure solution contained 7.3×10^{-2} mg Au, 9.8×10^{-2} mg Ag and 6.1×10^{-2} mg Pd. 0.5 mL of the nanodumbbell nanostructure solution contained 7.2×10^{-2} mg Au, 6.3×10^{-2} mg Ag and 6.2×10^{-2} mg Pd.

In-Situ Raman monitoring catalytic reaction: The in-Situ Raman monitoring catalytic reaction was carried out by the following approach. 1 mL of the as-synthesized AuNRs@AgPd dandelion nanostructures was centrifuged at 4000 rpm for 10 min, and then redispersed into 200 uL of ultra-filtered water. 100 uL of the above solution was added into a mixed solution of 2 mL 0.1 mM 4-nitrophenol (4-NTP) and 1 mL 0.1 M aqueous sodium borohydride ($NaBH_4$). The corresponding SERS spectra were recorded at 10s intervals directly on the solution under 632.8 nm laser excitation.

Instrumentation: TEM images were taken using a Tecnai G20 microscope (TEM, TecnaiG20, FEI company, US). HRTEM, STEM, SAED and EDS-mapping of images were performed using a Tecnai F20 microscope. XRD patterns were performed using a X'Pert PRO MPD system (PW3040/60, PANalytical, Holland) with Cu Ka radiation. XPS data was acquired using a Thermo ESCALAB 250Xi Multifunctional imaging electron spectrometer with a Al Kα source. Extinction spectra of all the samples were recorded using a UV-vis spectrometer (UV-3150, Shimadzu, Japan). The temperature was recorded through infrared thermal imaging system and imaged under a digital microscope (Leica Qwin). The Raman spectra were collected using a confocal microprobe Raman system (LabRam I, Dilor, France). The concentration of Au, Ag and Pd was determined using an inductively coupled plasma optical emission spectrometer (ICP-OES, Varian, 710-ES).

Acknowledgements

Notes and references

1   a) X. Xia, Y. Wang, A. Ruditskiy, Y. Xia, *Adv. Mate*. 2013, **25**, 6313; b) L. Zhou, Z. K. Liu, H. Zhang, S. Cheng, L-J Fan, W. L. Ma, *Nanoscale*, 2014, **6**, 12971; c) Y. Yu, Q. Zhang, J. Xie, J. Y. Lee, *Nat. Commun.* 2013, **4**, 1454; d) W. Zhang, J. Yang, X. Lu, *ACS Nano.* 2012, **6**, 7397; e) E. González, J. Arbiol, V. F. Puntes, *Science.* 2011, **334,** 1377; f) E. C. Cho, P. H. C. Camargo, Y. Xia, *Adv. Mater.* 2010, **22**, 744.

2   a) J. Chen, B. Wiley, J. McLellan, Y. Xiong, Z.-Y. Li, Y. Xia, *Nano Lett.* 2005, **5**, 2058; b) B. Goris, L. Polavarapu, S. Bals, G. Van Tendeloo, L. M. Liz-Marzán, *Nano Lett.* 2014, **14**, 3220; c) Y. Yang, J. Liu, Z. W. Fu, D. Qin, *J. Am. Chem. Soc.* 2014, **136**, 8153.

3   a) L. Weng, H. Zhang, A. O. Govorov, M. Ouyang, *Nat. Commun.* 2014, **5**, 4792; b) M. R. Buck, J. F. Bondi, R. E. Schaak, *Nat. Chem.* 2012, **4**, 37; c) F. Wang, S. Cheng, Z. Bao, J. Wang, *Angew. Chem. Int. Ed.* 2013, **52**, 10344; d) T. Mokari, C. G. Sztrum, A. Salant, E. Rabani, U. Banin, *Nat. Mater.* 2005,

4, 855; e) A. Walther, A. H. E. Müller, *Chem. Rev.* 2013, **113**, 5194. f) X. Pang, C. Wan, M. Wang, Z. Lin, *Angew. Chem. Int. Ed.* 2014, **53**, 5524.

4   a) J. Fennell, D.S. He, A.M. Tanyi, A.J, Logsdail, R.L. Johnston, Z.Y. Li, S.L. Horswell. *J. Am. Chem. Soc*. 2013, **135**, 6554. b) Y.J. Xiang, X.C. Wu , D.F. Liu, X.Y. Jiang, W.G. Chu, Z.Y. Li, Y. Ma, W.Y. Zhou, S.S. Xie, *Nano Lett.*, 2006, **6**, 2290. c) M. D. Xiao, C. M. Zhao, H. J. Chen, B. C. Yang, J. F. Wang, *Adv. Funct. Mater*. 2012, **22**, 4526. d) J. Li, J. Liu, Y. Yang, D. Qin, *J. Am. Chem. Soc.* 2015, **137**, 7039. e) L. Wang, Y. Yamauchi, *Chem. Mater.*, 2011, **23**, 2457. f) A. M. Henning, J. Watt, P. J. Miedziak, S. Cheong, M. Santonastaso, M. Song, Y. Takeda, A. I. Kirkland, S. H. Taylor and R. D. Tilley, *Angew. Chem., Int. Ed.*, 2013, **125,** 1517. g) F. Wang, C.h. Li, L.-D Sun, H.S. Wu, T. Ming, J.F. Wang, J. C. Yu, C.-H. Yan. *J. Am. Chem. Soc.*, 2011, **133**, 1106–1111. h) Q. Zhang, X. Guo, Z.X Liang, J.H Zeng, J. Yang, S.J. Liao. *Nano Res.*, 2013, **6**, 571-580.

5   R. Jiang, H. Chen, L. Shao, Q. Li, J. Wang, *Adv. Mater.* 2012, **24**, OP200.

6   a) Q. Zhang, X. Guo, Z.X. Liang, J.H. Zeng, J. Yang, S.J. Liao. *Nano Res.* 2013, **6**, 571-580. b) M.M Liu, Y.Z. Lu, W. Chen, *Adv. Func. Mater.* 2013, **23**, 1289-1296. c) X. B. Xie, G.H. Gao, S.D. Kang, T. Shibayama, Y.H. Lei, D.Y. Gao, L. T. Cai. *Adv. Mater.* 2015, **27,** 5573-5577. d) W.Q. Zhang, J.Z. Yang, X.M. Lu, *ACSnano.* 2012, **6,** 7397-7405. e) J.Y. Chen, B. Wiley, J. Mclellan, Y.J. Xiong, Z.-Y. Li, Y.N. Xia. *Nano Lett,* 2005, **5,** 2058-2062.

7   F. Wang, C. Li, L.-D. Sun, C.-H. Xu, J. Wang, J. C. Yu, C.-H. Yan, *Angew. Chem. Int. Ed.* 2012, **51**, 4872.

8   a) H. J. Jang, S. Ham, J. A. I. Acapulco, Y. Song, S. Hong, K. L. Shuford, S. Park, *J. Am. Chem. Soc.* 2014, **136**, 17674. b) H. Jing, H. Wang. *Chem. Mater.* 2015, **27**, 2172-2180.

9   Y. Xia, X. Xia, H. C. Peng, *J. Am. Chem. Soc.* 2015. DOI: 10.1021/ jacs.5b04641.

10 a) Z.R. Zhang, Z.N. Wang, S.N. He, C.Q. Wang, M.S. Jin, Y.D. Yin. *Chem. Sci.* 2015 DOI: 10.1039/C5SC01787D; b) Q.P. Lu, Z.D. Lu, Y.Z. Lu, L.F. Lv, Y. Ning, H.X. Yu , Y.B. Hou , Y.D. Yin, *Nano Lett.* 2013, **13**, 5698.

11 a) Q. Li, R. Jiang, T. Ming, C. Fang, J. Wang, *Nanoscale*. 2012, **4**, 7070. b) H. Chen, F. Wang, K. Li, K. C. Woo, J. Wang, Q. Li, L. D. Sun, X. Zhang, H. Q. Lin, C. H. Yan, *ACS Nano*. 2012, **6**, 7162.

12 a) W. Xie, B. Walkenfort, S. Schlücker, J. Am. Chem. Soc. 2013, 135, 1657; b) J. Huang, Y. Zhu, M. Lin, Q. Wang, L. Zhao, Y. Yang, K. X. Yao, Y. Han, *J. Am. Chem. Soc*. 2013, **135**, 8552.

Nanoscale Accepted Manuscript